Chemical composition of ambient PM$_{2.5}$ over China and relationship to precursor emissions during 2005–2012

Guannan Geng[1], Qiang Zhang[1], Dan Tong[1,2], Meng Li[1,2], Siwen Wang[2], and Kebin He[2]

[1]Ministry of Education Key Laboratory for Earth System Modeling, Department of Earth System Science, Tsinghua University, Beijing, China
[2]State Key Joint Laboratory of Environment Simulation and Pollution Control, School of Environment, Tsinghua University, Beijing, China

Correspondence to: Qiang Zhang (qiangzhang@tsinghua.edu.cn)

Abstract. We estimated the changes in chemical composition of ambient PM$_{2.5}$ over China during 2005–2012 using satellite-based aerosol optical depth (AOD) data and the GEOS-Chem chemical transport model, and investigated the driving forces behind the changes by examining the changes in precursor emissions using a bottom-up emission inventory. We found that the national population-weighted mean PM$_{2.5}$ concentration increased from 63.9 μg/m^3 in 2005 to 75.2 μg/m^3 in 2007, and subsequently decreased to 66.9 μg/m^3 from 2007 to 2012, composing a flat trend of population-weighted mean PM$_{2.5}$ concentration during 2005-2012. Variations in PM$_{2.5}$ concentrations are mainly driven by the changes in sulfate and nitrate concentrations. Population-weighted mean sulfate concentration increased by 10.7% from 2005–2006 (from 14.4 μg/m^3 to 15.9 μg/m^3) and then decreased by 4.3% per year from 2006–2012 (from 15.9 μg/m^3 to 12.9 μg/m^3), dominating the variations of total PM$_{2.5}$ concentrations. The decrease of sulfate concentration is partly offset by the increase of nitrate concentration: population-weighted mean nitrate concentration increased by 3.4% per year during 2005–2012 (from 9.8 μg/m^3 to 12.2 μg/m^3). The changes in sulfate and nitrate concentrations were in line with the changes in SO$_2$ and NO$_x$ emissions during the same period. By examining the emission data from the MEIC emission inventory, we found that the desulfurization regulation enforced around 2005 in power plants was the primary contributor to the SO$_2$ emissions reduction since 2006. In contrast, growth of energy consumption and lack of control measures for NO$_x$ resulted in persistent increase in NO$_x$ emissions until the installation of denitrification devices on power plants late in 2011, which began to take effect in 2012. The results of this work indicate that the synchronized abatement of emissions for multi-pollutants are necessary for reducing ambient PM$_{2.5}$ concentrations over China.

1 Introduction

Fine particulate matter with aerodynamic diameters of less than 2.5 μm (PM$_{2.5}$) is composed of a mixture of complex materials from multiple sources, including sulfate (SO$_4^{2-}$), nitrate (NO$_3^-$), ammonium (NH$_4^+$), black carbon (BC), organic mass (OM), crustal elements, and water. PM$_{2.5}$ and its chemical composition can penetrate deeply into human lungs and cause adverse health effects, including increased cardiovascular and respiratory morbidity and all-cause mortality (Dockery et al.,

1993; McDonnell et al., 2000; Pope et al., 2002). Some components (e.g., sulfate and BC) have significant impacts on the global energy budget system and are responsible for the direct climate effects of aerosols (IPCC, 2013). $PM_{2.5}$ can also trigger visibility degradation or haze events, which attract the public's attention.

Measurements of the historical trends in air quality represent the basis of health impact studies and control policy assessments. However, such datasets are usually limited in developing countries, including China. Indeed, before 2013, the Chinese national monitoring network did not report measurements of $PM_{2.5}$ or its chemical composition, and thus, it is difficult to elucidate the historical changes in aerosols and their driving forces across China. Air quality changes prior to 2013 have attracted substantial attention because China experienced rapid economic growth and urbanization during that time, along with increased energy demand. Additionally, the Chinese government has begun taking actions to mitigate emissions. Knowledge of the variations in the $PM_{2.5}$ chemical composition and their relationship to precursor emissions can be used to improve the design of future plans.

Previous studies focusing on historical $PM_{2.5}$ trend analysis typically depended on measurement data from several sites (He et al., 2001; Sun et al., 2015) or simulations using chemical transport models (CTMs) (Wang et al., 2013; Xing et al., 2015). Because of the substantial disparities in pollution characteristics between different regions in China, measurements from individual cities are insufficient to support a comprehensive national analysis or health impact study. CTMs can simulate the physical and chemical processes in the atmosphere and provide three-dimensional time-varying concentrations of air pollutants, which have been widely used in air quality studies (Wang et al., 2013; Xing et al., 2015). However, CTMs have limitations in $PM_{2.5}$ simulations, including missing precursors and formation mechanisms of secondary organic aerosols (Baek et al., 2011) and the lack of heterogeneous reactions, which may lead to underestimations of sulfate in haze events (Wang et al., 2014; Zheng et al., 2015). Therefore, a new method is needed to produce a spatially and temporally continuous historical dataset of $PM_{2.5}$ chemical compositions.

Satellite remote sensing of atmospheric pollutants has been widely used to understand the spatial and temporal distributions of air pollutants in recent years (Martin, 2008; Streets et al., 2013). Satellite retrievals can fill in the gaps in ground observations because of their high spatial and temporal coverage. Satellite remote sensing provides the column densities of trace gases (e.g., SO_2 and NO_2) and parameters that are related to aerosol concentrations, such as the aerosol optical depth (AOD), which has been widely used to estimate surface $PM_{2.5}$ concentrations (Chu et al., 2003; Wang and Christopher, 2003; van Donkelaar et al., 2016). Different types of methods can be used to retrieve ground-level $PM_{2.5}$ concentrations from satellite AOD data, including the use of CTMs to obtain conversion factors between $PM_{2.5}$ and AOD (Liu et al., 2004; van Donkelaar et al., 2010) and the use of statistical models (Hu et al., 2014; Zheng et al., 2016) or semi-empirical models (Lin et al., 2015; Zhang et al., 2015) to investigate the relationship among $PM_{2.5}$, AOD and other factors. Compared to statistical models and semi-empirical models, CTMs do not require ground measurements as input data and can also derive $PM_{2.5}$ composition concentrations (Philip et al., 2014), making them suitable for studies seeking to explore the historical $PM_{2.5}$ chemical composition prior to 2013 over China. Our previous work improved the method of retrieving $PM_{2.5}$ concentrations using CTMs over China (Geng et al., 2015), and the method is used in this study.

Atmospheric
Chemistry
and Physics
Discussions

In this study, we first attempted to fill in the gaps in PM$_{2.5}$ chemical composition measurements during 2005–2012 over China by using satellite AOD and conversion factors derived from a CTM, in addition to other correction factors. The satellite-based concentrations were then evaluated against ground measurements obtained from the literature. Based on satellite-derived datasets, we investigated the spatial and temporal variations of the PM$_{2.5}$ composition over China and

5 identified the dominant species involved in these variations. We further compared the chemical composition concentrations with precursor emissions to better understand their relationship and identify the driving forces behind the changes.

2 Methodology

2.1 Ground-based measurement data

As mentioned previously, national-scale PM$_{2.5}$ and chemical composition measurements are unavailable over China during

10 the study period (2005–2012). Therefore, we collected PM$_{2.5}$ and chemical composition measurements from the literature to evaluate our estimations. The sources, site locations, sampling period, and other information relevant to the collected data are summarized in Table S1. In total, we collected 94, 43, 43, 41, 50 and 52 records for PM$_{2.5}$, SO$_4^{2-}$, NO$_3^-$, NH$_4^+$, OC and BC, respectively. The collected measurements cover most of the eastern provinces, are randomly distributed in time, and are considered to be representative of our study time and region.

15 ### 2.2 Satellite-derived PM$_{2.5}$ and chemical composition concentrations

The satellite-derived PM$_{2.5}$ concentration datasets used in this work were adopted from Geng et al. (2015). These data were calculated using satellite AOD and conversion factors between AOD and PM$_{2.5}$ simulated by a CTM. Following Philips et al. (2014), the satellite-derived chemical compositions of PM$_{2.5}$ were estimated by applying composition-specific conversion factors to satellite AOD. The equations used for the PM$_{2.5}$ and composition calculations are:

20
$$\mathrm{PM}_{2.5,satellite} = \mathrm{AOD}_{satellite} \cdot \frac{\mathrm{PM}_{2.5,CTM}}{\mathrm{AOD}_{CTM}} \tag{1}$$

$$\mathrm{Composition}^k_{satellite} = \mathrm{AOD}_{satellite} \cdot \frac{\mathrm{Composition}^k_{CTM}}{\mathrm{AOD}_{CTM}} \tag{2}$$

where k represents different chemical compositions, including SO$_4^{2-}$, NO$_3^-$, NH$_4^+$, BC, OM, dust and sea salt, in this study. The AOD retrievals were provided by the Moderate Resolution Imaging Spectroradiometer (MODIS, Levy et al., 2007) and Multi-angle Imaging SpectroRadiometer (MISR, Kahn et al., 2007) instruments onboard the Terra satellite. Daily AOD data

25 from the two instruments were filtered against ground AOD measurements from the Aerosol Robotic Network (AERONET, Holben et al., 1998) and China Aerosol Remote Sensing NETwork (CARSNET, Che et al., 2009) before averaging them to reduce the uncertainties. We used the nested-grid GEOS-Chem model v9-01-02 (Bey et al., 2001; for more details, see the

Supporting Information) over Southeast Asia and year-by-year emission inventory over China to simulate the conversion factors between $PM_{2.5}$ species and AOD. The nested-grid model has a spatial resolution of 0.5° lat × 0.667° lon (Chen et al., 2009), which was driven by assimilated GEOS-5 meteorology from the Goddard Earth Observing System (GEOS) at the NASA Global Modeling and Assimilation Office (GMAO; http://gmao.gsfc.nasa.gov/). A total of eight years of simulations

5   were conducted with initialization on January 1, 2005 after a one-year spin-up simulation. The study time period (i.e., 2005–2012) could not be expanded because of the restrictions imposed by the GEOS-5 meteorology data. In addition, the aerosol vertical profiles from the space-based Cloud-Aerosol Lidar with Orthogonal Polarization (CALIOP, Winker et al., 2007) used to adjust the model simulations and corrections for incomplete sampling were also taken into account. More details are provided in Geng et al. (2015) and Philips et al. (2014).

10   The uncertainties associated with satellite-derived $PM_{2.5}$ compositions mainly relate to the satellite AOD retrievals, the modeled conversion factor between $PM_{2.5}$ and AOD, the modeled $PM_{2.5}$ composition fractions and incomplete sampling because of missing AOD data (Philip et al., 2014). Since the satellite AOD data were filtered against ground AOD measurements, the uncertainty of the AOD was restricted to the larger bound of ±20% or ±0.1. Vertical profiles from the CALIOP instrument were used to adjust the modeled profile; therefore, the uncertainties in the modeled $PM_{2.5}$/AOD ratio

15   were estimated as their annual mean differences. The normalized mean bias between each modeled component and ground observations was used as the error of the simulated $PM_{2.5}$ composition fraction. Uncertainty resulting from incomplete sampling was estimated as the relative difference between the modeled full-time mean value and the value coincidently sampled using satellite data. The total error was the sum of the described errors in quadrature.

2.3 Bottom-up emission inventory

20   The bottom-up emission information used in this study was taken from the Multi-resolution emission inventory for China (MEIC, http://www.meicmodel.org/). The MEIC model, which was developed and is maintained by Tsinghua University, is a technology-based, dynamic process emission model. The MEIC inventory is an update of the bottom-up emission inventory developed by the same group (Zhang et al., 2009) and includes estimated emissions from ~700 anthropogenic sources over China. The power sector was estimated using a unit-based dataset, and the spatial distribution of the power

25   emission was significantly improved (Wang et al., 2012; Liu et al., 2015). The on-road emissions were calculated using estimated county-level vehicle population data combined with an emission factor model (Zheng et al., 2014). We also built a framework to speciate the non-methane volatile organic compounds (NMVOCs) and provided model-ready NMVOC emissions for major chemical mechanisms (Li et al., 2014). In this work, the year-by-year emissions of SO_2, NO_x, NH_3, CO, OC, BC and NMVOCs during 2005–2012 were taken from the MEIC inventory as the GEOS-Chem model input to simulate

30   the conversion factors between $PM_{2.5}$ and AOD, and to support the emission driving force analysis.

In the bottom-up method, large uncertainties lie in the activity data, emission factors, removal efficiency and distribution of control technology, and spatial proxies (Zhang et al., 2009), which could affect the estimation of emission trends. To evaluate the estimated emission trends in the MEIC inventory, simulated tropospheric SO_2 and NO_2 columns from the

Atmospheric
Chemistry
and Physics
Discussions

GEOS-Chem model were compared with satellite observations from the Ozone Monitoring Instrument (OMI, Levelt et al., 2006). The satellite SO_2 products were taken from Wang et al. (2015), which were improved based on the standard NASA products to reduce uncertainties. The satellite NO_2 product was the OMI standard product, OMNO2 (version 2.1) (Bucsela et al., 2013). More descriptions of the satellite SO_2 and NO_2 columns are provided in the Supporting Information.

5   **3 Model Evaluation**

3.1 Satellite-derived concentration

Figure 1 compares the satellite-derived $PM_{2.5}$ and chemical composition concentrations with ground measurement data collected from the literature. Satellite-based data were extracted and averaged according to the corresponding sample period and location before comparison. All symbols were colored according to their site locations. Three regions covering most of

10   the anthropogenic sources over China were defined in this study as follows: Eastern China (ECN, 28–42°N, 110–123°E), the Pearl River Delta (PRD, 20–25°N, 110–117°E) and the Sichuan Basin (SCB, 27–33°N, 102–110°E). We found good agreement between the satellite-based and in situ $PM_{2.5}$ concentrations, with R = 0.72, slope = 0.80 and intercept = 10.18 µg/m^3. The chemical compositions estimated in this study also had good consistency with ground measurements, with R values in the range of 0.65-0.75 for different species. The satellite-derived data had relatively small biases in SO_4^{2-} and OM

15   estimations but overestimated NO_3^-, NH_4^+ and BC over polluted regions. The overestimation of NO_3^- and NH_4^+ was caused by overestimation of the NO_3^- fractions by the GEOS-Chem model, which was a common problem encountered in previous model studies (Park et al., 2004; Zhang et al., 2012; Wang et al., 2013). The overestimation of satellite-derived BC concentrations mainly occurred in the ECN region. However, the satellite-derived concentrations were improved relative to the model simulations (Figure S1).

20   **3.2 Modeled SO_2 and NO_2 columns**

To examine the model's capability for capturing the trends in $PM_{2.5}$ precursors, we also compared the normalized inter-annual trends of model-simulated and satellite-observed tropospheric SO_2 and NO_2 column densities over China, as shown in Figure 2. Satellite-derived NO_2 and SO_2 relative trends were well captured by the model simulations, with slight overestimation of the growth rates in some years. ECN had the best performance for both SO_2 and NO_2, with only a small

25   overestimation of the NO_2 growth rates during 2008–2009 and an underestimation of the SO_2 growth rate in 2007. The relative increases in the NO_2 columns were generally overestimated for PRD and SCB, indicating the possible overestimation of the NO_x emissions. The negative values in the satellite SO_2 columns over PRD were mainly caused by the strong interference of ozone absorption in the retrieval process, especially over clean regions where the SO_2 concentrations were low. However, the satellite-observed SO_2 columns showed a decreasing trend, which was consistent with the modeled

30   results.

Atmospheric
Chemistry
and Physics
Discussions

4 Results and Discussion

4.1 Spatiotemporal variations in the PM2.5 chemical composition

Figure 3 shows the multi-year mean spatial distributions of the satellite-derived $PM_{2.5}$ concentrations over China overlaid with ground measurements with sample periods exceeding one year during the corresponding timeframe. The spatial patterns
of $PM_{2.5}$ were well captured by the satellite-based data, with concentration enhancements of the anthropogenic pollution sources, including in the North China Plain, the Yangtze River Delta, the SCB and Hunan-Hubei province. The population-weighted mean mass concentrations of $PM_{2.5}$ over China were in the range of 63.9–75.2 μg/m^3 during 2005–2012 and were nearly twice the Chinese national standard. China had an overall negative $PM_{2.5}$ trend of 0.3% per year during 2005–2012; a positive trend of 18.2% per year was observed in 2005–2007, followed by a negative trend of 2.7% per year in 2008–2012.
According to the inter-annual $PM_{2.5}$ changes over China shown in Figure 4a, the $PM_{2.5}$ level exhibited a general downward trend after the peak year (2007), although a slight rebound of the $PM_{2.5}$ concentration was observed in 2011. The $PM_{2.5}$ trend estimated in this work was consistent with those of previous studies (Boys et al., 2014; Ma et al., 2015).

The inter-annual changes in the $PM_{2.5}$ concentrations for ECN, PRD and SCB are presented in Figure 4b-4d. Regional disparities were found in the time series of $PM_{2.5}$ concentrations, especially at the inflection points beginning decreases or
rebounds. ECN's trend was similar to the national trend, whereas in the PRD, a persistent negative trend of 2.6 μg/m^3 per year in $PM_{2.5}$ after 2007 was observed, with no rebound. $PM_{2.5}$ levels in the SCB peaked in 2006, which was one year before the national peak; subsequently, it increased again beginning in 2008 until decreasing in 2012.

The spatial distributions and time series of secondary inorganic aerosols (sulfate, nitrate and ammonium [SNA]) are shown in Figure 5. The spatial patterns of SNA in the eastern part of China were similar to those of $PM_{2.5}$. Satellite-based data could
well reproduce the regional heterogeneity of SNA, although NO_3^- was overestimated over ECN. The sulfate concentrations over eastern China generally exceeded 15.0 μg/m^3, and the highest values occurred in the SCB ($\geq$ 30 μg/m^3). Regarding the nitrate concentrations, the highest values were observed in the North China Plain, reflecting the different emission characteristics of sulfate and nitrate. SNA showed quite different temporal variations relative to the total $PM_{2.5}$. The population-weighted mean sulfate concentrations over China showed a negative trend of 2.4% per year during the study
period (from 14.4 μg/m^3 in 2005 to 12.9 μg/m^3 in 2012), as shown in Figure 5j, with a peak value in 2006 (15.9 μg/m^3) and a rebound in 2011 (Figure 4e). In contrast to SO_4^{2-}, the nitrate concentrations over China had an increasing trend of 3.4% per year (from 9.8 μg/m^3 in 2005 to 12.2 μg/m^3 in 2012), which partially compensated for the reduction in sulfate and caused the total $PM_{2.5}$ to drop one year after sulfate. In 2012, nitrate decreased for the first time, and sulfate decreased again, causing the total $PM_{2.5}$ to decline as well. The temporal trends of sulfate and nitrate also differed among the three regions. ECN and SCB
had SO_4^{2-} trends similar to the national trend, whereas in the PRD, the SO_4^{2-} concentrations decreased consistently after 2007. The SCB had a larger NO_3^- growth rate compared to other regions, which could explain the earlier rebound of $PM_{2.5}$ in this region.

Atmospheric
Chemistry
and Physics
Discussions

Figure 6 presents the spatial and temporal changes of carbonaceous aerosols. Satellite-based data performed well for estimating OM concentrations but tended to overestimate the BC concentrations in polluted regions. The OM concentrations were highlighted in densely populated regions because organic carbon is mainly produced by residential combustion. BC hotspots were most apparent in populous regions and large cities, consistent with previous ground observation studies (Cao et al., 2007). Negative trends of 0.9% and 0.1% per year were found for OM and BC, respectively, and these trends held nearly steady over this period.

The spatial and temporal changes in mineral dust and sea salt are presented in Figure 7. High values of mineral dust (exceeding 80.0 $\mu g/m^3$) were found over the desert regions (e.g., the Taklimakan Desert), which were the largest contributors to $PM_{2.5}$ in northwestern China. Sea salt was mainly distributed along the coast, and its concentrations were less than 1.0 $\mu g/m^3$. Dust and sea salt were mainly produced from natural sources and fluctuated during this period.

Based on the analysis described above, we found that sulfate and nitrate were the two dominant components driving the variations in the $PM_{2.5}$ concentration during 2005–2012. Decreases in SO_4^{2-} caused the total $PM_{2.5}$ concentrations to decline beginning in 2007, whereas NO_3^- was the main reason for the $PM_{2.5}$ rebound observed in 2011. We also compared the relative abundances of nitrate and sulfate (i.e., NO_3^-/SO_4^{2-}) in different years to confirm the variations of these two species. The NO_3^-/SO_4^{2-} ratio over China was generally less than 2, lower than the values reported for developed cities (e.g., 2–5 in Los Angeles, Kim et al., 2000). The NO_3^-/SO_4^{2-} ratios were larger in the eastern part of China, which had higher vehicle populations (Zheng et al., 2014), and in western China (e.g., Sichuan, Chongqing, and Ningxia), where coal with higher sulfur contents is burned (Tang et al., 2008), resulting in higher emission factors of SO_2. During 2005–2012, the NO_3^-/SO_4^{2-} ratios over China exhibited a distinct increasing trend, further supporting the changes in the relative abundances of sulfate and nitrate in the atmosphere. Thus, the contribution of the mobile sector to $PM_{2.5}$ increased, while the contribution from point sources decreased. Ground measurements also reflected the increasing trend in the NO_3^-/SO_4^{2-} ratio over China. For example, Fu et al. (2014) found that the NO_3^-/SO_4^{2-} ratio in Guangzhou increased from 0.31 to 0.69 during 2007–2011. Additionally, Tan et al. (2016) observed an increase in the NO_3^-/SO_4^{2-} ratio from 0.73 to 0.92 in Foshan during 2008–2012.

4.2 Relationship between the $PM_{2.5}$ composition and precursor emissions

The sulfate and nitrate concentrations were compared with the precursor emissions of SO_2 and NO_x to elucidate the driving forces underlying the changes in the $PM_{2.5}$ components, as shown in Figure 8. We used the percent changes relative to the 2005 benchmark for the direct comparison of the concentrations and emissions. The relative changes in the SO_2 and NO_x emissions were consistent with the changes in the sulfate and nitrate concentrations, respectively, although discrepancies were noted in the growth and reduction rates.

Atmospheric
Chemistry
and Physics
Discussions

On the national scale, the relative changes in SO_4^{2-} from 2005 to 2012 corresponded almost linearly to the relative changes in SO_2 emissions, whereas the relative increase in NO_3^- during 2005–2012 was less than that of NO_x emissions. During this time period, NH_3 emissions remained steady, and the magnitude was less than the sum of the SO_2 and NO_x emissions on a molecular basis, indicating that NH_3-limited conditions existed in China. Although the decrease of SO_4^{2-} released free NH_3 in

5   a 1:2 ratio, the amount of NH_3 released could not fully neutralize the increased nitric acid because the increase in the NO_x emissions was more than twice the decrease in the SO_2 emissions (e.g., an 11% reduction in SO_2 emissions vs. a 48% increase in NO_x emissions in 2012). This explains why the relative increase of NO_3^- was less than that of NO_x emissions (e.g., a 24% increase of NO_3^- in 2012).

Among the three regions, the PRD had the largest reduction rates of SO_2 emissions and the lowest growth rates of NO_x

10   emissions, consistent with the faster decline of SO_4^{2-} concentrations and slower increase of NO_3^- concentrations in this region. The SCB had a larger growth rate of NO_x emissions compared to other regions, which could explain the rapid increase of NO_3^- concentrations. Differences were observed in the relative change rates of SO_4^{2-} concentrations and SO_2 emissions. Possible explanations for these differences include uncertainties in the bottom-up SO_2 emission trend, as described in Sect. 3.2, and the influences of the varying meteorological conditions over the years. Similar to the national trend, the growth of

15   the NO_3^- concentration was not only affected by the NO_x emission increase but also by changes in the SO_4^{2-} concentrations via the thermodynamic equilibrium of SNA.

Figure 9 presents the inter-annual emission trends of SO_2 and NO_x in four sectors taken from the MEIC inventory. We also established a hypothetical scenario of emission trends that assumed that the emission factors and technology distributions remained unchanged during 2005–2012 to separate the effects of activity (A) and emission factor (EF) changes. The

20   hypothetical scenario represented the emission changes caused by A changes alone, and the differences between the hypothetical scenario and the actual emissions reflected the emission changes caused by EF variations.

As shown in Figure 9, the total SO_2 emissions peaked in 2006 (34.3 Tg) and subsequently decreased. This reduction was mainly driven by the power sector, which is a major source of SO_2 emissions over China. China set a target to reduce national SO_2 emissions by 10% in the 11th Five Year Plan (FYP, 2006–2010) and took corresponding actions, including the

25   mandatory installation of flue-gas desulfurization (FGD) in coal-fired power plants and the optimization of generation unit fleets by promoting large power plants and decommissioning small plants (The State Council of the People's Republic of China 2006). Although the increasing electricity demand tended to increase SO_2 emissions by 68% during 2005–2011, the reduced SO_2 EFs completely reversed the SO_2 emissions in the power sector, causing them to decrease at a rate of 1.4 Tg/yr and confirming the success of FGD operation and the optimization of the mix of generation unit fleets. After reaching a

30   bottom value of 28.4 Tg in 2010, the SO_2 emissions subsequently increased. This rebound was mainly caused by the growing activity rates in the industrial sector and limited control measures in iron and steel production. Therefore, successful control

Atmospheric
Chemistry
and Physics
Discussions

of SO_2 emissions in the power sector was the key factor relating to SO_4^{2-} reduction after 2007, whereas limited controls in the industrial sector contributed to the SO_4^{2-} rebound.

The total NO_x emissions over China showed completely different trends compared to SO_2 emissions because of the distinct control processes implemented for SO_2 and NO_x by the Chinese government. China established a goal to reduce NO_x emissions by 10% late in the 12th FYP (2011–2015) and pursued the installation of selective catalytic reduction (SCR) equipment at power plants beginning in 2011. Previously, the control measures on NO_x in the power sector were limited, whereas the energy demand increased continuously, leading to a dramatic increase in NO_x emissions from the power sector during 2005–2011. Meanwhile, the Chinese government promoted the construction of precalciner kilns, which are the most energy-efficient cement kilns, to replace the shaft kilns for cement production. However, the NO_x EF increased because the higher operational temperatures and more automated air-flow systems of precalciner kilns resulted in higher NO_x emissions compared to shaft kilns. In the transport sector, NO_x emissions increased by 19.3% in 2012 relative to 2005; this value was the result of a 17.4% decline because of the implementation of staged regulations and a 36.7% increase attributed to vehicle population growth. In comparison to 2011, a decline in the activity level in the power sector in 2012 caused a 26.5-Gg NO_x emissions reduction, much less than the emission reduction of 897.5 Gg, indicating that SCR promotion began to take effect.

The rapid increase of NO_x emissions caused the NO_3^- concentrations to rise, compensating for the reductions in the SO_4^{2-} concentration and even leading to a rebound in the $PM_{2.5}$ concentration.

Figure 10 summarizes the region-specific by-sector emission change rates caused by A and EF changes, which could facilitate understanding the regional disparities in $PM_{2.5}$ composition variations. ECN exhibited emission patterns that were very similar to those observed at the national level, and the SO_2 control measures implemented in the power sector were most effective in ECN. Indeed, in this region, a reduction rate of 17.4% per year was attributed to the EF reduction, larger than those observed in the PRD (11.4%/year) and SCB (9.9%/year). The PRD had more effective control of power sector NO_x emissions, and the vehicle population in this region grew more slowly, contributing to slower growth of the total NO_x emission and, thus, persistent $PM_{2.5}$ reduction after 2007. In the SCB, coal consumption in the industrial sector grew quickly, and as a result, the SO_2 and NO_x emissions increased by 20.9% and 20.0% per year, respectively. Reductions in the sulfur content of the coal burned in the SCB reduced the SO_2 EFs and offset a large fraction of the increased emissions. In contrast, for NO_x emissions, the EFs continued to increase, causing the NO_x emissions and NO_3^- concentrations over the SCB to increase dramatically.

4.3 Uncertainties and limitations

The national population-weighted mean uncertainties were estimated to be 3.4 µg/m³ for sulfate, 2.7 µg/m³ for nitrate, 2.0 µg/m³ for ammonium, 1.2 µg/m³ for BC and 4.6 µg/m³ for OM. Despite the large uncertainties in the magnitudes of the estimated $PM_{2.5}$ compositions, the trend analysis performed here was relatively unaffected because most of the uncertainties were systematic errors, and we used the normalized trend to cancel out most of them. The bottom-up emissions used to

Atmospheric
Chemistry
and Physics
Discussions

elucidate the driving forces were also expected to include large uncertainties, but we focused on the emission trend, which could be more reliable. In addition, we used a CTM and satellite observations from the OMI instrument to further support the estimated precursor emissions, which increased the robustness of our study.

Another limitation of our study is that the influence of meteorological conditions was not considered. Indeed, meteorological

5   parameters, such as temperature, humidity and precipitation, influence the gas-phase formation of sulfate, gas-to-aerosol partitioning, and the wet and dry depositions of aerosols, which all contribute to the inter-annual variations in the $PM_{2.5}$ concentrations. According to Mu and Liao (2014), $PM_{2.5}$ concentrations exhibit large inter-annual variations in North China, especially during winter, when the meteorological parameters vary greatly. Indeed, North China had larger inter-annual variations in summer, whereas the SCB exhibited the smallest inter-annual variations among the polluted regions. In this

10   work, we used annual mean values to compare concentrations and emissions, which might have partially reduced the variation of the uncertainties between seasons. However, future work is needed to more accurately quantify the relationship between precursor emissions and aerosol concentrations.

5 Concluding Remarks

In this study, we estimated the chemical compositions of ambient $PM_{2.5}$ over China during 2005–2012, a period for which

15   national ground measurements are unavailable. The method used to derive the dataset was adopted from previous studies (Philip et al., 2014; Geng et al., 2015) and involved satellite AOD data from the MODIS and MISR instruments, conversion factors taken from the nested-grid GEOS-Chem model and other correction factors. Good agreement was found between the estimated concentrations and ground measurements obtained from the literature.

We studied the spatiotemporal variations of $PM_{2.5}$ compositions over China based on satellite-derived datasets and sought to

20   identify the driving forces underlying these changes. The national population-weighted mean $PM_{2.5}$ concentration increased relative to 2005, peaked in 2007, and subsequently decreased, except for a rebound in 2011. Of the three polluted regions studied here, the PRD was the only one to exhibit a persistent decrease in $PM_{2.5}$ after 2007; other regions had different peak and rebound years. The decline in the total $PM_{2.5}$ concentrations after 2007 was mainly attributable to sulfate reduction, whereas the rebound in $PM_{2.5}$ in 2011 was caused by persistent nitrate growth and a rebound in the sulfate concentration. The

25   ratios between nitrate and sulfate increased over China from 2005 to 2012, further confirming the relative abundance changes of these two species.

Bottom-up emission inventories of the precursors SO_2 and NO_x were examined to explain the variations in these species. FGD operation in the power sector was the primary contributor to SO_2 reduction, whereas the growth of industrial emissions caused SO_2 emissions to rebound in 2011. Limited control measures implemented during 2005–2011 caused the NO_x

30   emissions to increase rapidly, whereas the SCR system installed in the power sector during the 12th FYP caused the NO_x emissions to decline in 2012. The SO_2 and NO_x emission trends were generally consistent with the sulfate and nitrate

concentrations, respectively, but exhibited different relative change rates, which could be explained by the thermodynamic equilibrium of SNA.

This study's findings show that the simultaneous regulation of SO_2 and NO_x is crucial for $PM_{2.5}$ mitigation in China. A recent study (Cheng et al., 2016) reported that NO_x is not only a precursor for nitrate but is also an important oxidant

5   contributing to sulfate formation in northern China. This finding highlights the importance of controlling NO_x emissions. The government has already implemented stricter control measures to reduce SO_2 and NO_x emissions in recent years. FGD devices have been promoted in iron and steel production to reduce industrial SO_2 emissions, and the use of SCR devices in the power sector also resulted in significant effects, causing the trend in NO_x emissions to decline since 2011 (de Foy et al., 2016; Liu et al., 2016; van Der A et al., 2016). Ground measurements from the national monitoring network established in

10   2013 demonstrate a decreasing trend in $PM_{2.5}$ over China since 2013, confirming the efficacy of the emissions controls implemented in China. In the future, more attention should be paid to curbing NO_x emissions.

Acknowledgements

15   **References**

Baek, J., Hu, Y., Odman, M. T., and Russell, A. G.: Modeling secondary organic aerosol in CMAQ using multigenerational oxidation of semi-volatile organic compounds, J. Geophys. Res., 116, D22204, 2011.

Bey, I., Jacob, D. J., Yantosca, R. M., Logan, J. A., Field, B. D., Fiore, A. M., Li, Q. B., Liu, H. G. Y., Mickley, L. J., and Schultz, M. G.: Global modeling of tropospheric chemistry with assimilated meteorology: Model description and evaluation,

20   J. Geophys. Res., 106, 23073-23095, 2001.

Boys, B. L., Martin, R. V., van Donkelaar, A., MacDonell, R. J., Hsu, N. C., Cooper, M. J., Yantosca, R. M., Lu, Z., Streets, D. G., Zhang, Q., and Wang, S. W.: Fifteen-Year Global Time Series of Satellite-Derived Fine Particulate Matter, Environ. Sci. Technol., 48, 11109-11118, 2014.

Bucsela, E. J., Krotkov, N. A., Celarier, E. A., Lamsal, L. N., Swartz, W. H., Bhartia, P. K., Boersma, K. F., Veefkind, J. P.,

25   Gleason, J. F., and Pickering, K. E.: A new stratospheric and tropospheric NO_2 retrieval algorithm for nadir-viewing satellite instruments: applications to OMI, Atmos. Meas. Tech., 6, 2607-2626, 2013.

Cao, J., Lee, S., Chow, J. C., Watson, J. G., Ho, K., Zhang, R., Jin, Z., Shen, Z., Chen, G., and Kang, Y.: Spatial and seasonal distributions of carbonaceous aerosols over China, J. Geophys. Res., 112, 2007.

Che, H., Zhang, X., Chen, H., Damiri, B., Goloub, P., Li, Z., Zhang, X., Wei, Y., Zhou, H., Dong, F., Li, D., and Zhou, T.: Instrument calibration and aerosol optical depth validation of the China Aerosol Remote Sensing Network, J. Geophys. Res., 114, D03206, 2009.

Chen, D., Wang, Y., McElroy, M. B., He, K., Yantosca, R. M., and Le Sager, P.: Regional CO pollution and export in China simulated by the high-resolution nested-grid GEOS-Chem model, Atmos. Chem. Phys., 9, 3825-3839, 2009.

Cheng, Y., Zheng, G., Wei, C., Mu, Q., Zheng, B., Wang, Z., Gao, M., Zhang, Q., He, K., and Carmichael, G.: Reactive nitrogen chemistry in aerosol water as a source of sulfate during haze events in China, Sci. Adv., 2, e1601530, 2016.

Chu, D. A., Kaufman, Y. J., Zibordi, G., Chern, J. D., Mao, J., Li, C. C., and Holben, B. N.: Global monitoring of air pollution over land from the Earth Observing System-Terra Moderate Resolution Imaging Spectroradiometer (MODIS), J. Geophys. Res., 108, 2003.

de Foy, B., Lu, Z., and Streets, D. G.: Satellite NO_2 retrievals suggest China has exceeded its NO_x reduction goals from the twelfth Five-Year Plan, Scientific Reports, 6, 2016.

Dockery, D. W., Pope, C. A., Xu, X. P., Spengler, J. D., Ware, J. H., Fay, M. E., Ferris, B. G., and Speizer, F. E.: An association between air-pollution and mortality in 6 Uinited-States cities, New Engl. J. Med., 329, 1753-1759, 1993.

Fu, X., Wang, X., Guo, H., Cheung, K., Ding, X., Zhao, X., He, Q., Gao, B., Zhang, Z., Liu, T., and Zhang, Y.: Trends of ambient fine particles and major chemical components in the Pearl River Delta region: Observation at a regional background site in fall and winter, Sci. Total Environ., 497–498, 274-281, 2014.

Geng, G., Zhang, Q., Martin, R. V., van Donkelaar, A., Huo, H., Che, H., Lin, J., and He, K.: Estimating long-term $PM_{2.5}$ concentrations in China using satellite-based aerosol optical depth and a chemical transport model, Remote Sens. Environ., 166, 262-270, 2015.

He, K. B., Yang, F. M., Ma, Y. L., Zhang, Q., Yao, X. H., Chan, C. K., Cadle, S., Chan, T., and Mulawa, P.: The characteristics of $PM_{2.5}$ in Beijing, China, Atmos. Environ., 35, 4959-4970, 2001.

Holben, B. N., Eck, T. F., Slutsker, I., Tanre, D., Buis, J. P., Setzer, A., Vermote, E., Reagan, J. A., Kaufman, Y. J., Nakajima, T., Lavenu, F., Jankowiak, I., and Smirnov, A.: AERONET - A federated instrument network and data archive for aerosol characterization, Remote Sens. Environ., 66, 1-16, 1998.

Hu, X., Waller, L. A., Lyapustin, A., Wang, Y., Al-Hamdan, M. Z., Crosson, W. L., Estes Jr, M. G., Estes, S. M., Quattrochi, D. A., Puttaswamy, S. J., and Liu, Y.: Estimating ground-level $PM_{2.5}$ concentrations in the Southeastern United States using MAIAC AOD retrievals and a two-stage model, Remote Sens. Environ., 140, 220-232, 2014.

IPCC: Climate Change 2013: The Physical Science Basis: Summary for Policymakers, Cambridge, UK, 2013.

Kahn, R. A., Li, W. H., Moroney, C., Diner, D. J., Martonchik, J. V., and Fishbein, E.: Aerosol source plume physical characteristics from space-based multiangle imaging, J. Geophys. Res., 112, 2007.

Kim, B. M., Teffera, S., and Zeldin, M. D.: Characterization of $PM_{2.5}$ and PM_{10} in the South Coast Air Basin of Southern California: Part 1—Spatial Variations, J. Air Waste Manag. Assoc., 50, 2034-2044, 2000.

Atmospheric
Chemistry
and Physics
Discussions

Levelt, P. F., Van den Oord, G. H. J., Dobber, M. R., Malkki, A., Visser, H., de Vries, J., Stammes, P., Lundell, J. O. V., and Saari, H.: The Ozone Monitoring Instrument, IEEE T. Geosci. Remote Sens., 44, 1093-1101, 2006.

Levy, R. C., Remer, L. A., Mattoo, S., Vermote, E. F., and Kaufman, Y. J.: Second-generation operational algorithm: Retrieval of aerosol properties over land from inversion of Moderate Resolution Imaging Spectroradiometer spectral

5 reflectance, J. Geophys. Res., 112, 2007.

Li, M., Zhang, Q., Streets, D. G., He, K. B., Cheng, Y. F., Emmons, L. K., Huo, H., Kang, S. C., Lu, Z., Shao, M., Su, H., Yu, X., and Zhang, Y.: Mapping Asian anthropogenic emissions of non-methane volatile organic compounds to multiple chemical mechanisms, Atmos. Chem. Phys., 14, 5617-5638, 2014.

Lin, C., Li, Y., Yuan, Z., Lau, A. K. H., Li, C., and Fung, J. C. H.: Using satellite remote sensing data to estimate the high-

10 resolution distribution of ground-level $PM_{2.5}$, Remote Sens. Environ., 156, 117-128, 2015.

Liu, F., Zhang, Q., Tong, D., Zheng, B., Li, M., Huo, H., and He, K. B.: High-resolution inventory of technologies, activities, and emissions of coal-fired power plants in China from 1990 to 2010, Atmos. Chem. Phys., 15, 13299-13317, 2015.

Liu, F., Zhang, Q., Zheng, B., Tong, D., Yan, L., Zheng, Y., and He, K.: Recent reduction in NO_x emissions over China: synthesis of satellite observations and emission inventories, Environ. Res. Lett., 11, 114002, 2016.

15 Liu, Y., Park, R. J., Jacob, D. J., Li, Q. B., Kilaru, V., and Sarnat, J. A.: Mapping annual mean ground-level $PM_{2.5}$ concentrations using Multiangle Imaging Spectroradiometer aerosol optical thickness over the contiguous United States, J. Geophys. Res., 109, 2004.

Ma, Z., Hu, X., Sayer, A. M., Levy, R., Zhang, Q., Xue, Y., Tong, S., Bi, J., Huang, L., and Liu, Y.: Satellite-Based Spatiotemporal Trends in PM Concentrations: China, 2004-2013, Environ. Health Perspect., 24, 24, 2015.

20 Martin, R. V.: Satellite remote sensing of surface air quality, Atmos. Environ., 42, 7823-7843, 2008.

McDonnell, W. F., Nishino-Ishikawa, N., Petersen, F. F., Chen, L. H., and Abbey, D. E.: Relationships of mortality with the fine and coarse fractions of long-term ambient PM_{10} concentrations in nonsmokers, J. Expo. Anal. Environ. Epidemiol., 10, 427-436, 2000.

Mu, Q. and Liao, H.: Simulation of the interannual variations of aerosols in China: role of variations in meteorological

25 parameters, Atmos. Chem. Phys. Discuss., 14, 11177-11219, 2014.

Murray, L. T., Jacob, D. J., Logan, J. A., Hudman, R. C., and Koshak, W. J.: Optimized regional and interannual variability of lightning in a global chemical transport model constrained by LIS/OTD satellite data, J. Geophys. Res., 117, D20307, 2012.

Park, R. J., Jacob, D. J., Field, B. D., Yantosca, R. M., and Chin, M.: Natural and transboundary pollution influences on

30 sulfate-nitrate-ammonium aerosols in the United States: Implications for policy, J. Geophys. Res., 109, 2004.

Philip, S., Martin, R. V., van Donkelaar, A., Lo, J. W.-H., Wang, Y., Chen, D., Zhang, L., Kasibhatla, P. S., Wang, S., Zhang, Q., Lu, Z., Streets, D. G., Bittman, S., and Macdonald, D. J.: Global Chemical Composition of Ambient Fine Particulate Matter for Exposure Assessment, Environ. Sci. Technol., 48, 13060-13068, 2014.

Pope, C. A., Burnett, R. T., Thun, M. J., Calle, E. E., Krewski, D., Ito, K., and Thurston, G. D.: Lung cancer, cardiopulmonary mortality, and long-term exposure to fine particulate air pollution, Jama-J. Am. Med. Assoc., 287, 1132-1141, 2002.

Streets, D. G., Canty, T., Carmichael, G. R., de Foy, B., Dickerson, R. R., Duncan, B. N., Edwards, D. P., Haynes, J. A.,

5 Henze, D. K., Houyoux, M. R., Jacob, D. J., Krotkov, N. A., Lamsal, L. N., Liu, Y., Lu, Z., Martin, R. V., Pfister, G. G., Pinder, R. W., Salawitch, R. J., and Wecht, K. J.: Emissions estimation from satellite retrievals: A review of current capability, Atmos. Environ., 77, 1011-1042, 2013.

Sun, Y. L., Wang, Z. F., Du, W., Zhang, Q., Wang, Q. Q., Fu, P. Q., Pan, X. L., Li, J., Jayne, J., and Worsnop, D. R.: Long-term real-time measurements of aerosol particle composition in Beijing, China: seasonal variations, meteorological effects,

10 and source analysis, Atmos. Chem. Phys., 15, 10149-10165, 2015.

Tan, J., Duan, J., Ma, Y., He, K., Cheng, Y., Deng, S.-x., Huang, Y.-l., and Si-Tu, S.-p.: Long-term trends of chemical characteristics and sources of fine particle in Foshan City, Pearl River Delta: 2008–2014, Sci. Total Environ., 565, 519-528, 2016.

Tang, S., Sun, S., Qin, Y., Jiang, Y., and Wang, W.: Distribution characteristics of sulfur and the main harmful trace

15 elements in China's coal, Acta. Geol. Sin-Engl. Ed., 82, 722-730, 2008.

van der A, R. J., Mijling, B., Ding, J., Koukouli, M. E., Liu, F., Li, Q., Mao, H., and Theys, N.: Cleaning up the air: Effectiveness of air quality policy for SO_2 and NO_x emissions in China, Atmos. Chem. Phys. Discuss., 2016, 1-18, 2016.

van Donkelaar, A., Martin, R. V., Brauer, M., Hsu, N. C., Kahn, R. A., Levy, R. C., Lyapustin, A., Sayer, A. M., and Winker, D. M.: Global Estimates of Fine Particulate Matter using a Combined Geophysical-Statistical Method with Information from

20 Satellites, Models, and Monitors, Environ. Sci. Technol., 50, 3762-3772, 2016.

van Donkelaar, A., Martin, R. V., Brauer, M., Kahn, R., Levy, R., Verduzco, C., and Villeneuve, P. J.: Global Estimates of Ambient Fine Particulate Matter Concentrations from Satellite-Based Aerosol Optical Depth: Development and Application, Environ. Health Perspect., 118, 847-855, 2010.

Wang, J. and Christopher, S. A.: Intercomparison between satellite-derived aerosol optical thickness and $PM_{2.5}$ mass:

25 Implications for air quality studies, Geophys. Res. Lett., 30, 2003.

Wang, S., Zhang, Q., Martin, R. V., Philip, S., Liu, F., Li, M., Jiang, X., and He, K.: Satellite measurements oversee China's sulfur dioxide emission reductions from coal-fired power plants, Environ. Res. Lett., 10, 2015.

Wang, S. W., Zhang, Q., Streets, D. G., He, K. B., Martin, R. V., Lamsal, L. N., Chen, D., Lei, Y., and Lu, Z.: Growth in NO_x emissions from power plants in China: bottom-up estimates and satellite observations, Atmos. Chem. Phys., 12, 4429-

30 4447, 2012.

Wang, Y., Zhang, Q., Jiang, J., Zhou, W., Wang, B., He, K., Duan, F., Zhang, Q., Philip, S., and Xie, Y.: Enhanced sulfate formation during China's severe winter haze episode in January 2013 missing from current models, J. Geophys. Res., 119, 2013JD021426, 2014.

Wang, Y., Zhang, Q. Q., He, K., Zhang, Q., and Chai, L.: Sulfate-nitrate-ammonium aerosols over China: response to 2000-2015 emission changes of sulfur dioxide, nitrogen oxides, and ammonia, Atmos. Chem. Phys., 13, 2635-2652, 2013.

Winker, D. M., Hunt, W. H., and McGill, M. J.: Initial performance assessment of CALIOP, Geophys. Res. Lett., 34, L19803, 2007.

Xing, J., Mathur, R., Pleim, J., Hogrefe, C., Gan, C. M., Wong, D. C., Wei, C., Gilliam, R., and Pouliot, G.: Observations and modeling of air quality trends over 1990–2010 across the Northern Hemisphere: China, the United States and Europe, Atmos. Chem. Phys., 15, 2723-2747, 2015.

Zhang, L., Jacob, D. J., Knipping, E. M., Kumar, N., Munger, J. W., Carouge, C. C., van Donkelaar, A., Wang, Y. X., and Chen, D.: Nitrogen deposition to the United States: distribution, sources, and processes, Atmos. Chem. Phys., 12, 4539-4554, 2012.

Zhang, Q., Streets, D. G., Carmichael, G. R., He, K. B., Huo, H., Kannari, A., Klimont, Z., Park, I. S., Reddy, S., Fu, J. S., Chen, D., Duan, L., Lei, Y., Wang, L. T., and Yao, Z. L.: Asian emissions in 2006 for the NASA INTEX-B mission, Atmos. Chem. Phys., 9, 5131-5153, 2009.

Zhang, Y. and Li, Z.: Remote sensing of atmospheric fine particulate matter ($PM_{2.5}$) mass concentration near the ground from satellite observation, Remote Sens. Environ., 160, 252-262, 2015.

Zheng, B., Huo, H., Zhang, Q., Yao, Z. L., Wang, X. T., Yang, X. F., Liu, H., and He, K. B.: High-resolution mapping of vehicle emissions in China in 2008, Atmos. Chem. Phys., 14, 9787-9805, 2014.

Zheng, B., Zhang, Q., Zhang, Y., He, K. B., Wang, K., Zheng, G. J., Duan, F. K., Ma, Y. L., and Kimoto, T.: Heterogeneous chemistry: a mechanism missing in current models to explain secondary inorganic aerosol formation during the January 2013 haze episode in North China, Atmos. Chem. Phys., 15, 2031-2049, 2015.

Zheng, Y., Zhang, Q., Liu, Y., Geng, G., and He, K.: Estimating ground-level $PM_{2.5}$ concentrations over three megalopolises in China using satellite-derived aerosol optical depth measurements, Atmos. Environ., 124, Part B, 232-242, 2016.
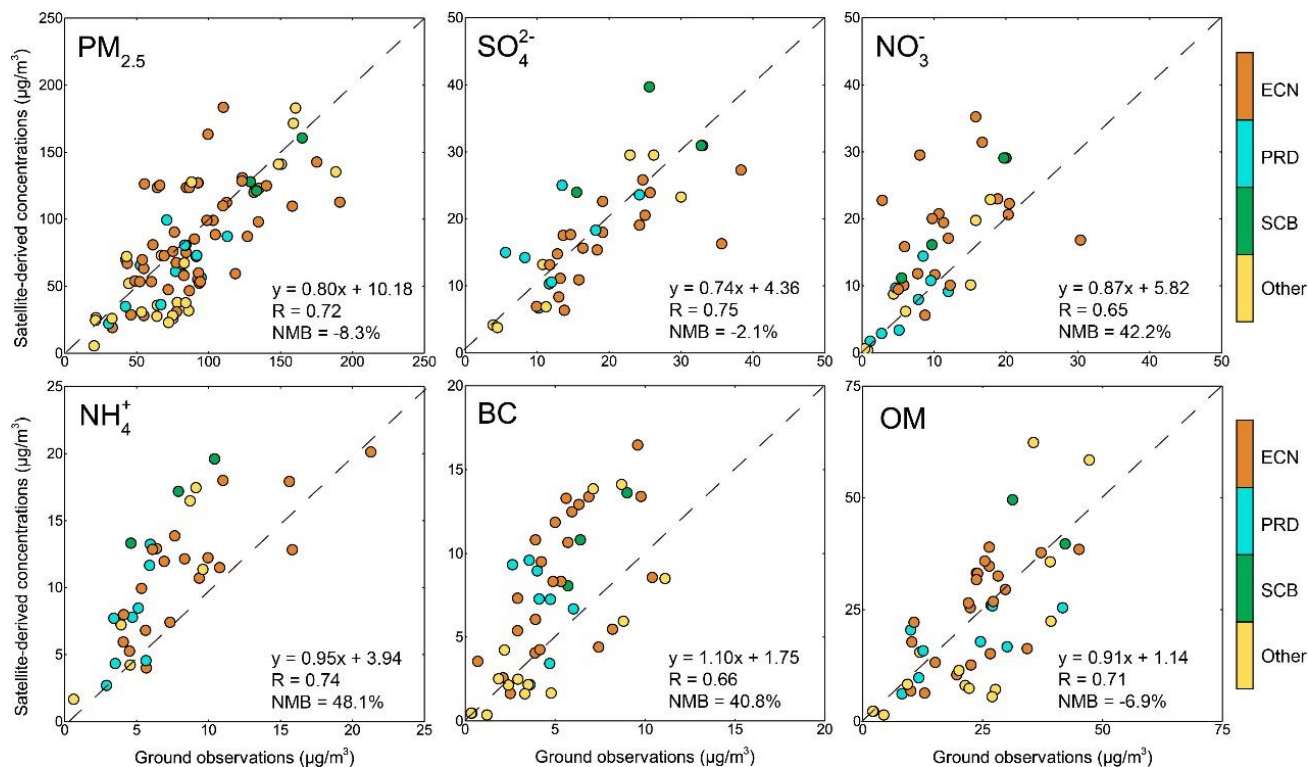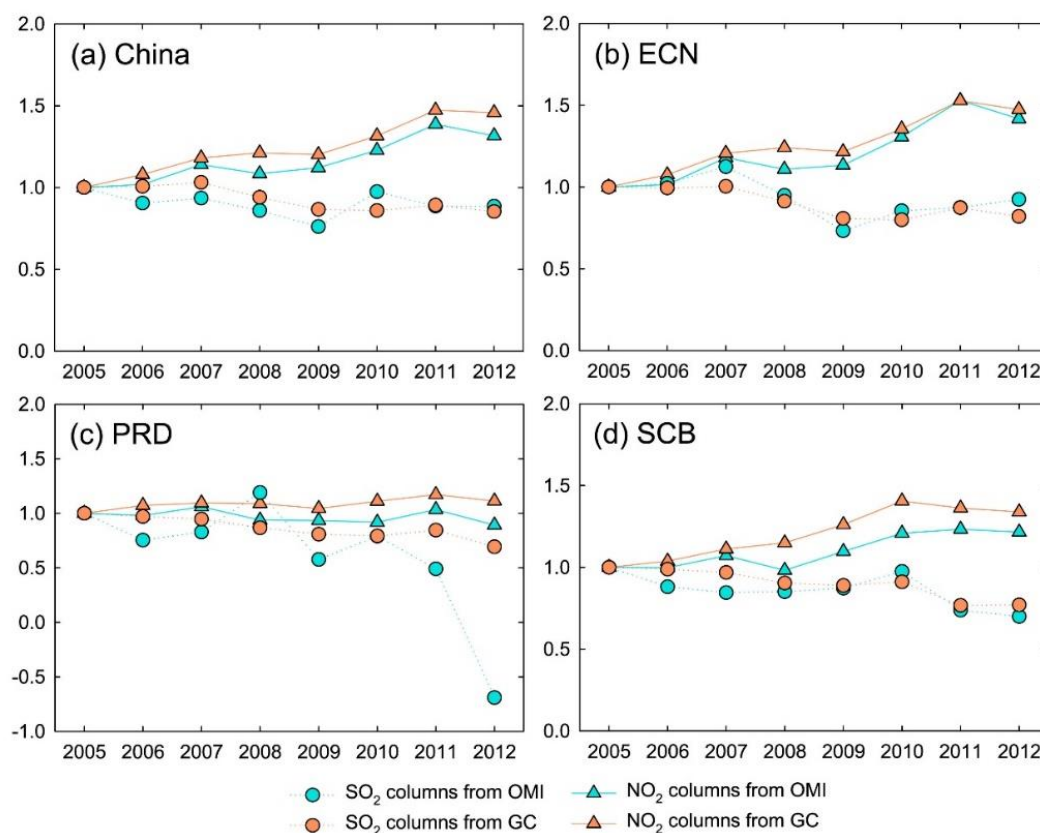
Atmospheric
Chemistry
and Physics
Discussions

Figure 1. Evaluation of satellite-derived PM₂.₅ and chemical composition concentrations using in situ data collected from the literature. The colors of the symbols represent the locations of the collected in situ data. The three defined regions are ECN (28–42°N, 110–123°E), PRD (20–25°N, 110–117°E) and SCB (27–33°N, 102–110°E). The dashed line corresponds to the 1:1 line in each panel.

Figure 2. The inter-annual trends of the simulated and observed tropospheric column densities for SO₂ and NO₂ over (a) China, (b) ECN, (c) PRD and (d) SCB during 2005–2012. All data are normalized by the value in 2005. The dotted lines with circles denote SO₂, and the solid lines with triangles denote NO₂. Cyan and orange represent the satellite (OMI) and model (GC) values, respectively.
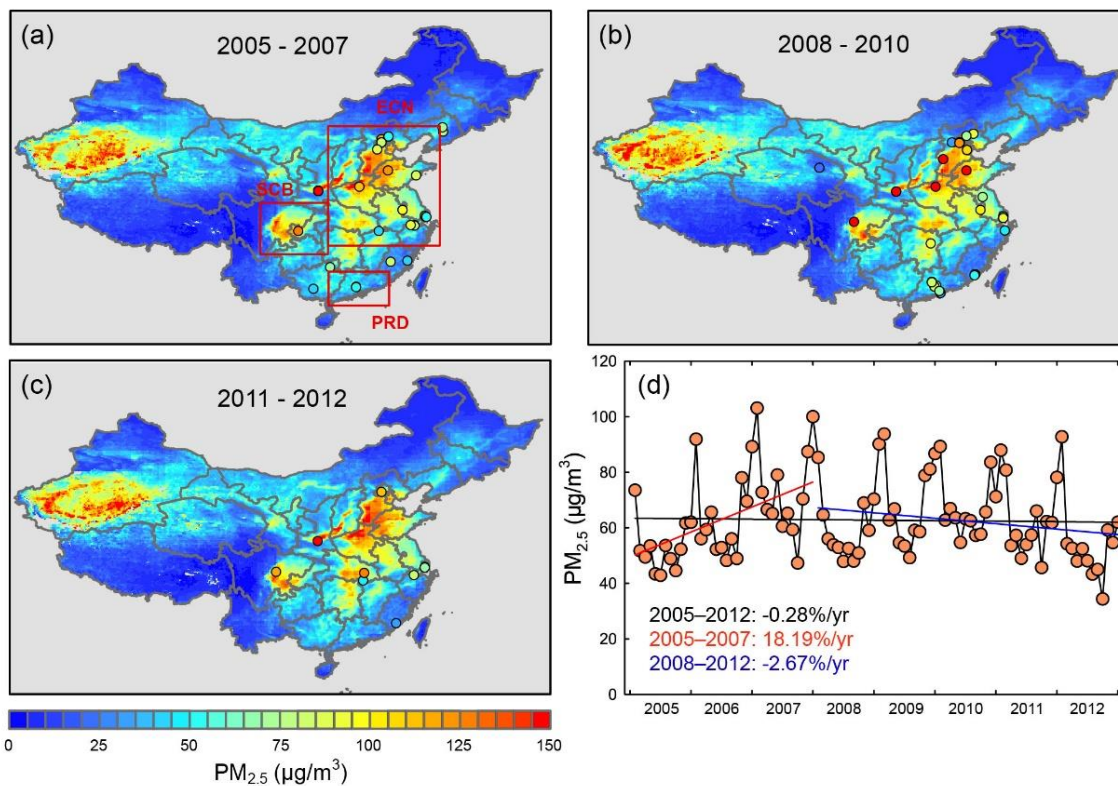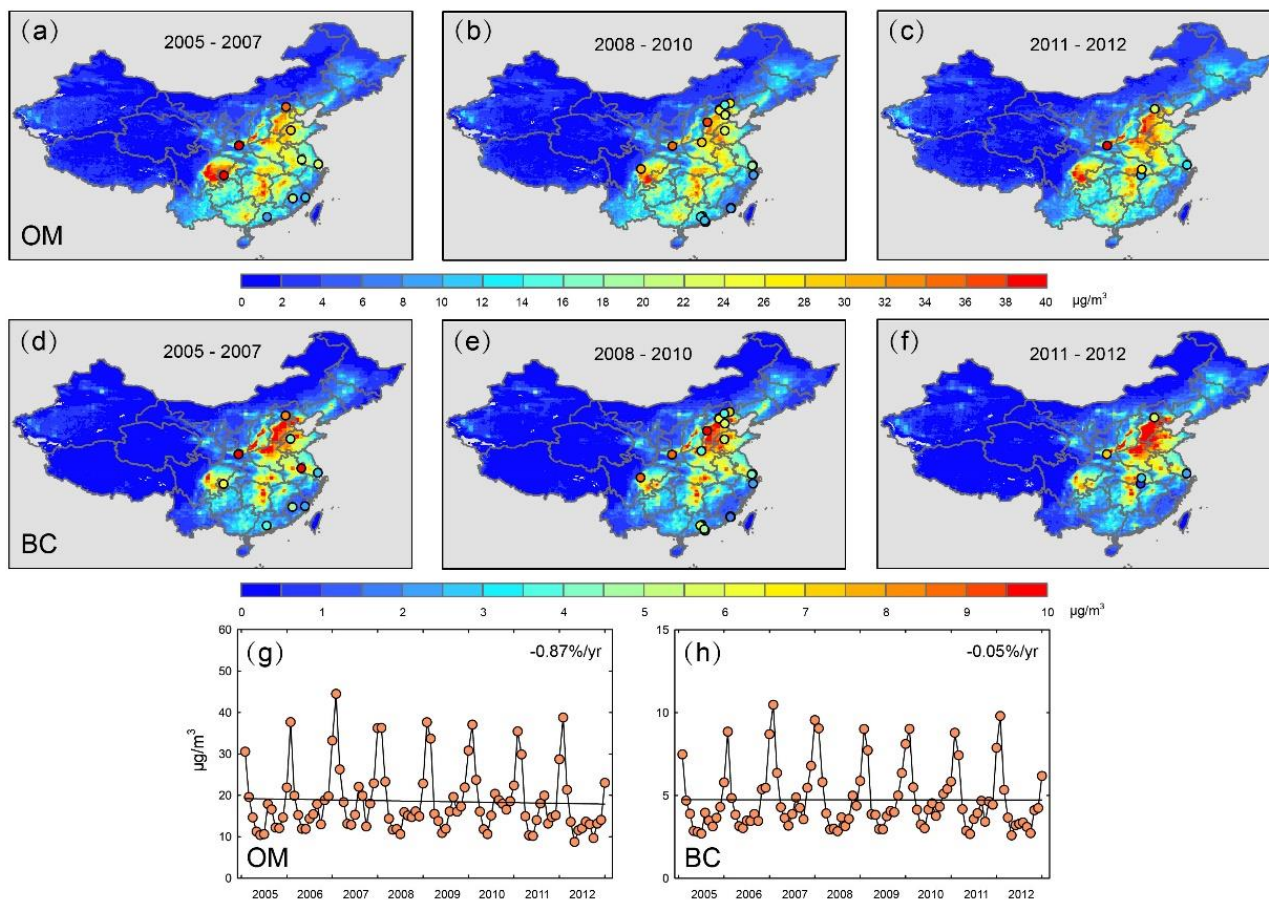
Figure 3. Spatial distributions of averaged PM₂.₅ over China during (a) 2005–2007, (b) 2008–2010 and (c) 2011–2012 overlaid with ground measurements collected during the corresponding time period. (d) The population-weighted monthly mean PM₂.₅ concentrations over China and their regression trend. Boxed areas outline the regions defined in this study.
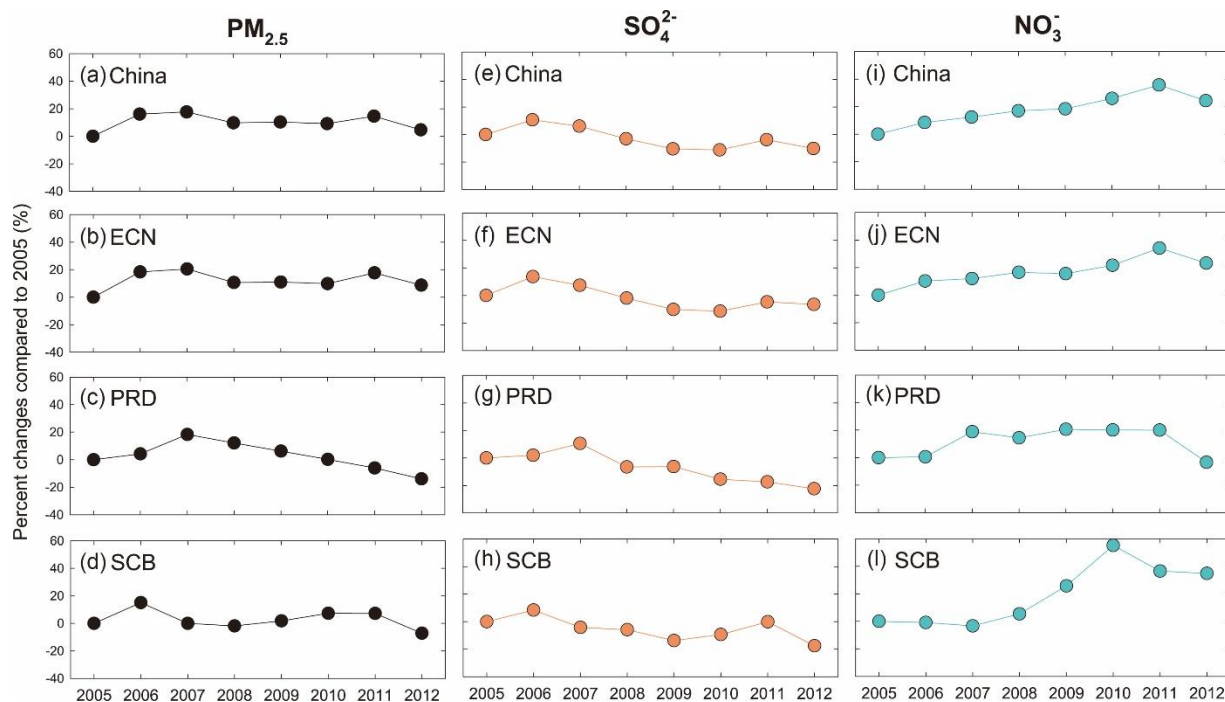
Figure 4. Inter-annual percent changes of (a-d) PM$_{2.5}$, (e-h) SO$_4^{2-}$ and (i-l) NO$_3^-$ concentrations compared to 2005 over China, ECN, PRD and SCB.
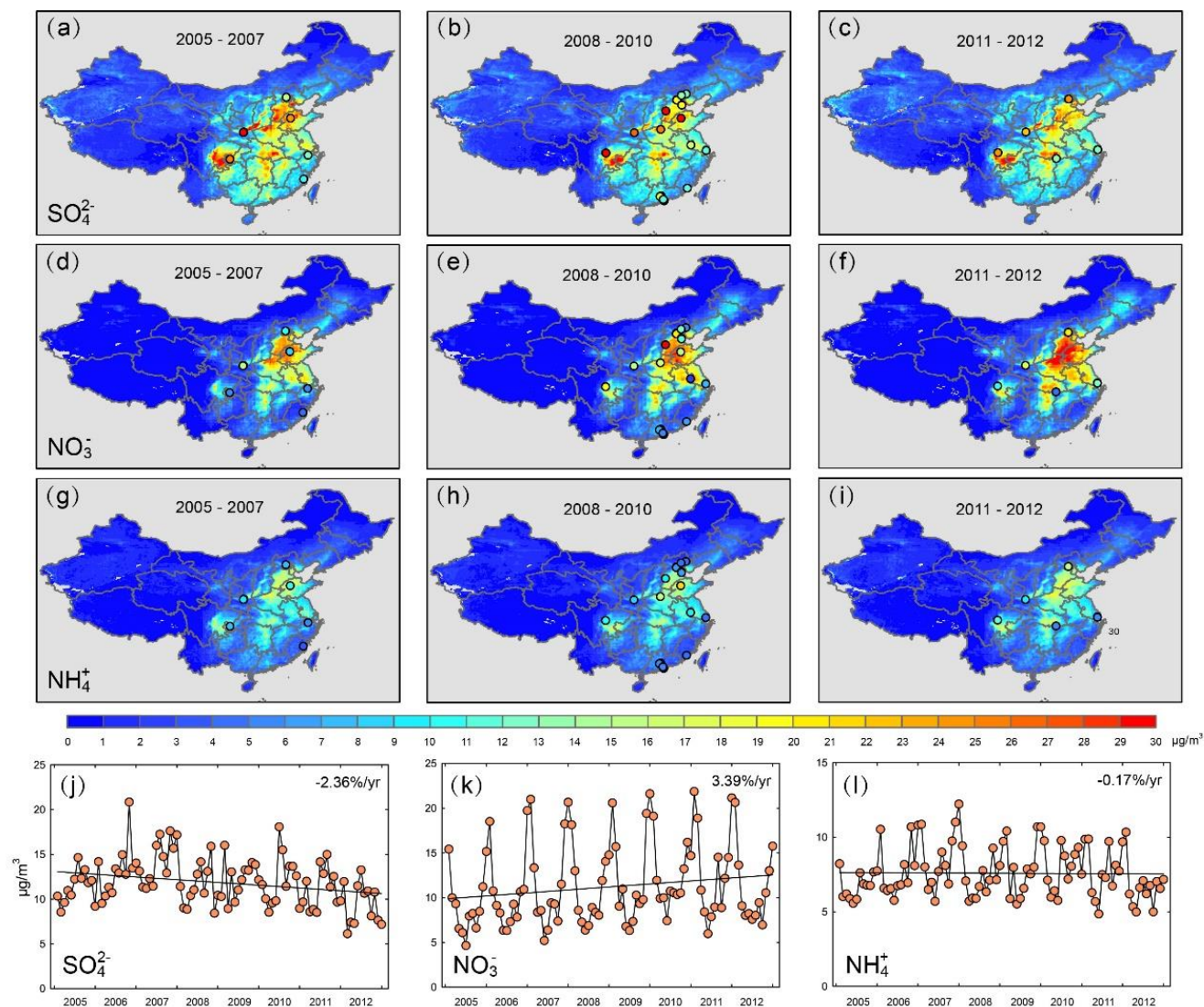
Figure 5. Spatial distributions of averaged (a-c) SO_4^{2-}, (d-f) NO_3^- and (g-i) NH_4^+ over China during 2005–2007, 2008–2010 and 2011–2012 overlaid with ground measurements collected during the corresponding time period. (j-l) The population-weighted monthly mean SO_4^{2-}, NO_3^- and NH_4^+ concentrations over China and their regression trends.

5

Figure 6. Spatial distributions of averaged (a-c) OM and (d-f) BC over China during 2005–2007, 2008–2010 and 2011–2012 overlaid with ground measurements collected during the corresponding time period. (g-h) The population-weighted monthly mean OM and BC concentrations over China and their regression trends.
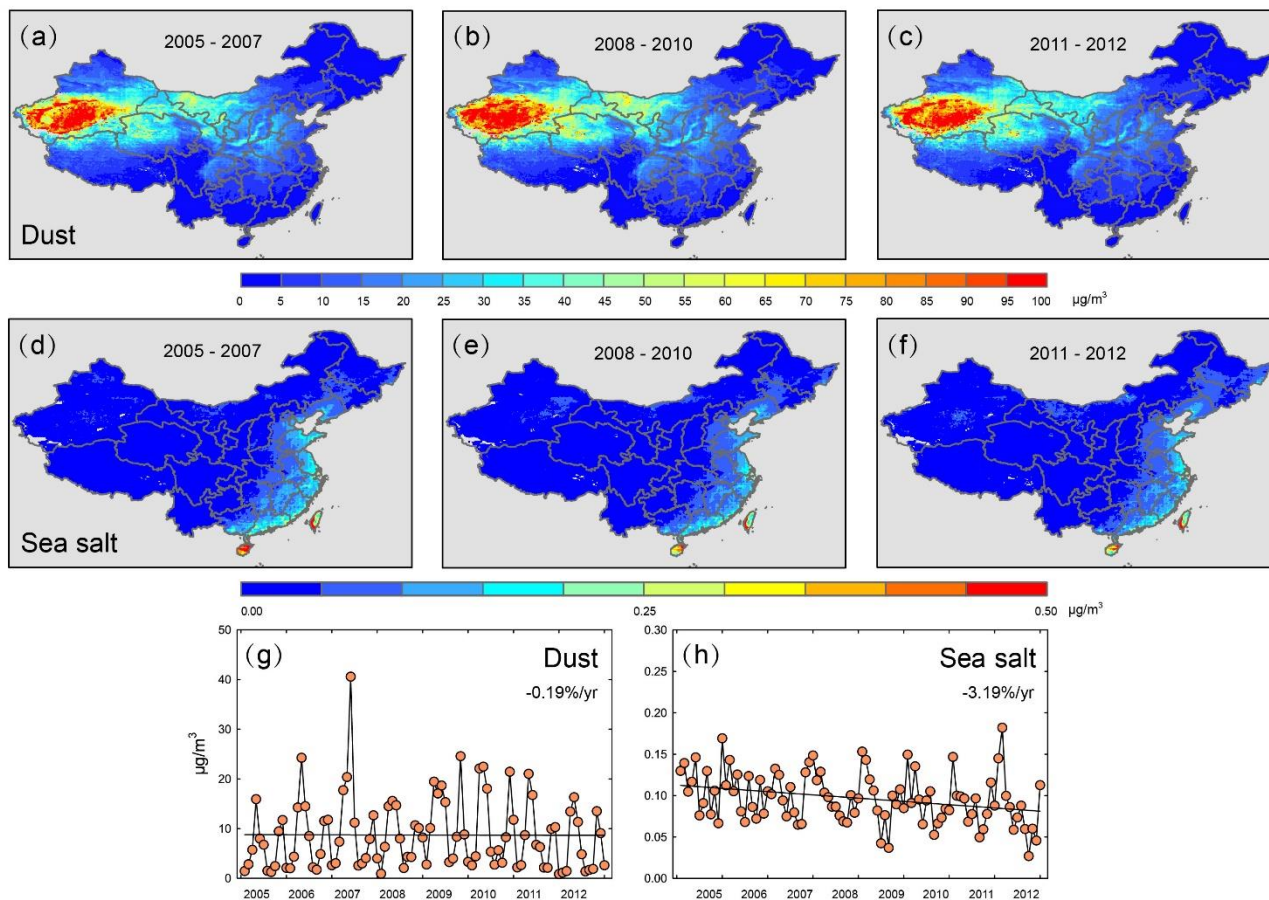
5

Atmospheric
Chemistry
and Physics
Discussions

Figure 7. Spatial distributions of averaged (a-c) dust and (d-f) sea salt over China during 2005–2007, 2008–2010 and 2011–2012. (g-h) The population-weighted monthly mean dust and sea salt concentrations over China and their regression trends.
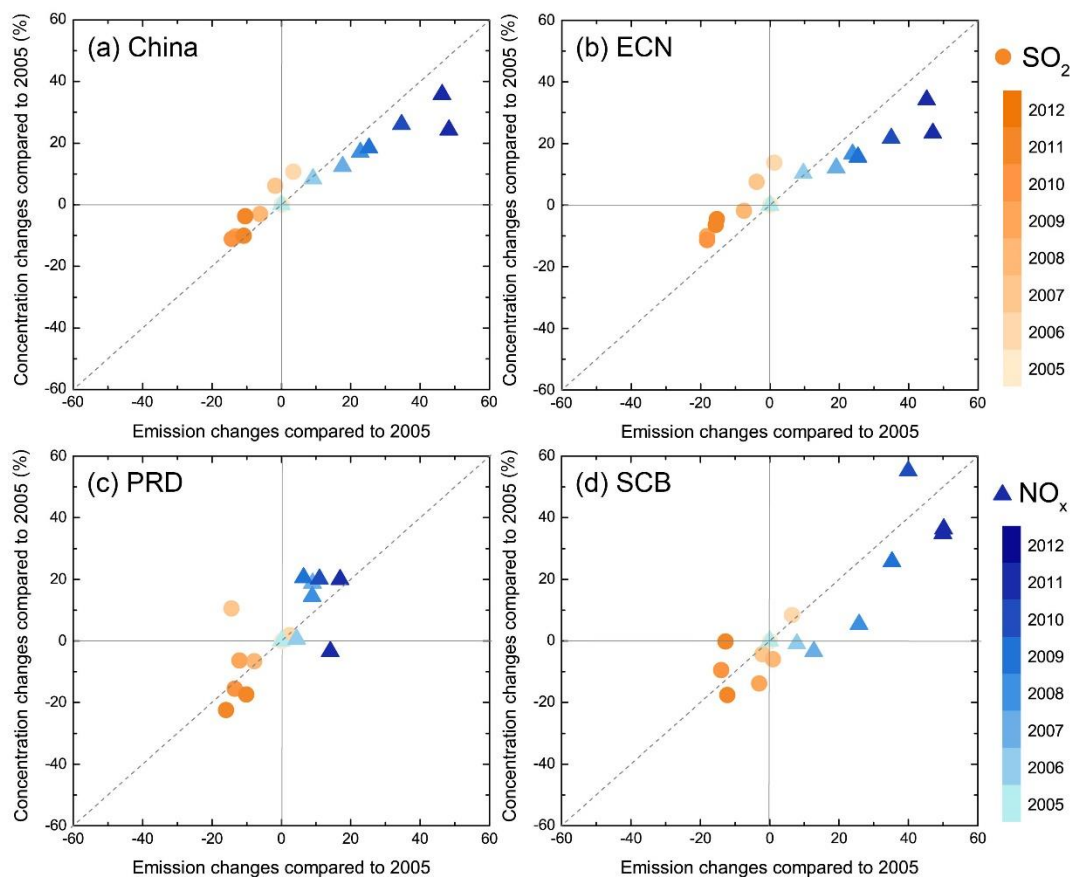
5

Figure 8. Comparisons of changes in the SO_4^{2-} and NO_3^- mass concentrations and their precursor emissions during 2005–2012. All data are presented as percent changes relative to 2005. The oranges circles and blue triangles represent SO_4^{2-} and NO_3^-, respectively, and the shades of the symbols' colors denote the year.

5

Atmospheric
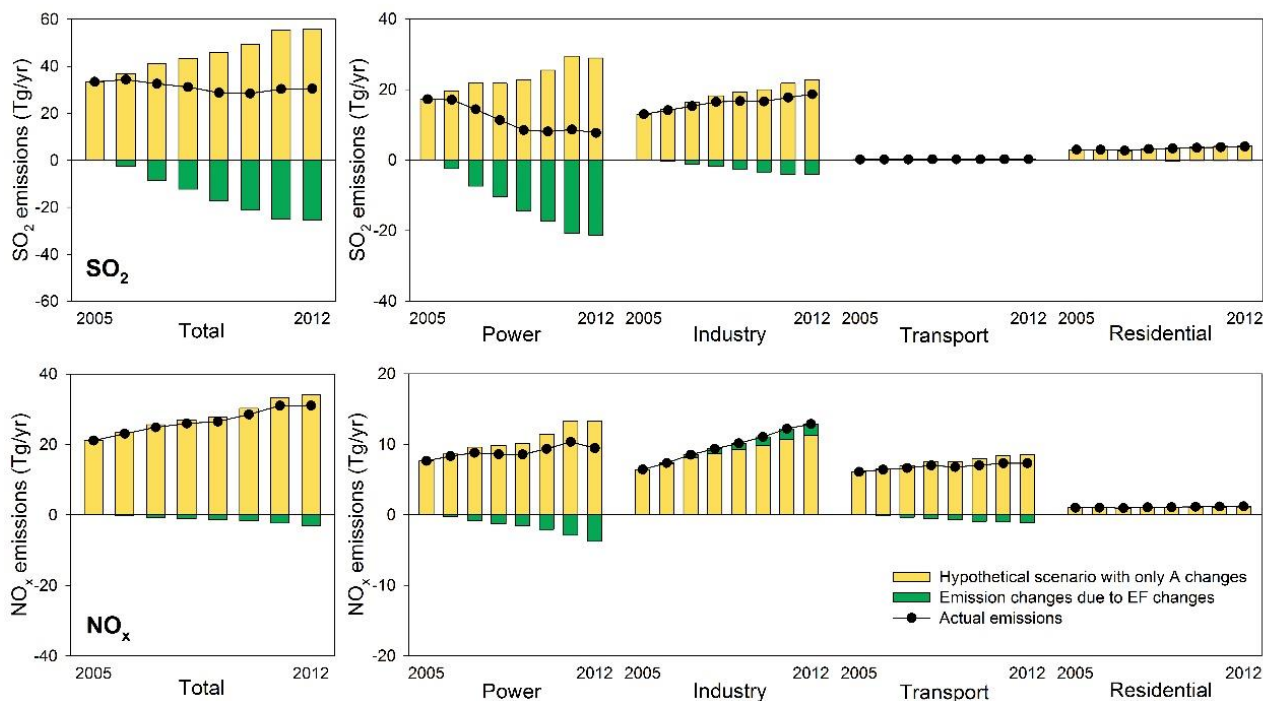Chemistry
and Physics
Discussions

Open Access

EGU

Figure 9. SO₂ and NOₓ emissions by sector during 2005–2012 over China. The black circles denote the actual inter-annual emission trends estimated using the MEIC inventory. The yellow bars represent the hypothetical scenario involving only activity (A) changes. The green bars indicate the emission changes resulting from variations in the emission factor (EF). The top row illustrates the SO₂ emissions, and the bottom row presents the NOₓ emissions.

Atmospheric
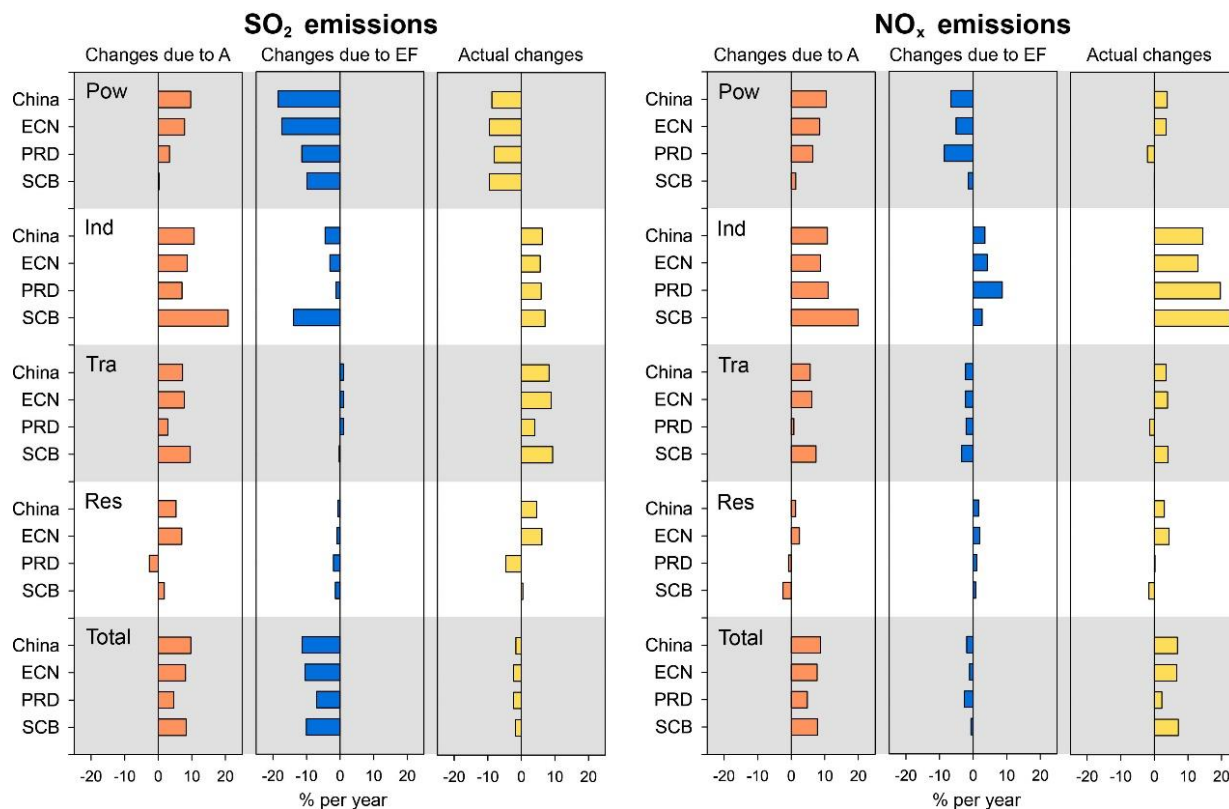Chemistry
and Physics
Discussions

Open Access

Figure 10. Summary of the average emission changes (% per year) during 2005–2012 for the power (Pow), industry (Ind), transport (Tra) and residential (Res) sectors over China and the three regions. Orange bars indicate the emission changes caused by activity (A) changes, and blue bars represent the emission changes caused by emission factor (EF) changes. Yellow bars present the actual emission changes estimated using the MEIC model.